Materials Chemistry and Physics 348 (2026) 131713

Contents lists available at ScienceDirect

Materials Chemistry and Physics

journal homepage: www.elsevier.com/locate/matchemphys

$SrCoO_{3-\delta}$ and $SrCo_{1-x}Ti_xO_{3-\delta}$ perovskites as electrocatalytic materials for oxygen evolution reaction in alkaline environment

Valentina Maria Volanti [a,1], Anastasiia Semenova [b,1], Andrea Zaffora [c,*], Monica Santamaria [c], Ilia Valov [b,d,e,f,**]

[a] Department of Applied Science and Technology, Politecnico di Torino, Corso Duca degli Abruzzi 24, 10129, Torino, Italy
[b] Institute for Materials in Electrical Engineering and Information Technology (IWE 2), RWTH Aachen University, 52074, Aachen, Germany
[c] Department of Engineering, University of Palermo, Viale delle Scienze, Ed. 6, 90128, Palermo, Italy
[d] JARA – Fundamentals of Future Information Technology, Forschungszentrum Jülich, 52425, Jülich, Germany
[e] Institute of Electrochemistry and Energy System, Forschungszentrum Jülich, 52425, Jülich, Germany
[f] "Acad. Evgeni Budevski" IEE-BAS, Bulgarian Academy of Sciences (BAS), Akad. G. Bonchev 10, 1113, Sofia, Bulgaria

HIGHLIGHTS

- $SrCoO_{3-\delta}$ thin films deposited by chemical bath deposition.
- Co excess improves OER activity, Ti doping enhances durability.
- Best sample shows η_{onset} = 284 mV and Tafel slope = 59 mV dec^{-1}.
- Ti reduces Sr leaching, stabilizing perovskite electrocatalysts.

ARTICLE INFO

Keywords:
Perovskites
OER
Water electrolysis
Ti doping
Strontium cobaltite

ABSTRACT

Here, we report the deposition of $SrCoO_{3-\delta}$ perovskites thin films by chemical bath deposition, employed as electrocatalytic layers for oxygen evolution reaction (OER) in alkaline water splitting. The effect of Co excess and Ti-doping on the crystalline structure, composition and electrochemical performances was investigated. The former had effect only on electrochemical performance whilst Ti-doping, above 3 %, induced the formation of a secondary phase. Among all the investigated samples, $SrCoO_{3-\delta}$:Co_3O_4 (SCO:CB) sample showed the best electrochemical performance toward OER in 1 M KOH aqueous solution, reporting an onset overpotential, η_{onset}, of 284 mV and a Tafel slope of 59 mV dec^{-1}. In contrast, Ti-doping (i.e. 3 %, SCT:CB 3 sample) drastically improved stability of the electrocatalytic layer, enabling 24 h of continuous operation, demonstrating the effectiveness of doping strategy to enhance $SrCoO_{3-\delta}$ perovskites durability. XPS analyses revealed that degradation of electrochemical performance of thin films is related to Sr leaching, even if Ti-doping decreased leached Sr amount improving layers stability.

1. Introduction

The growing of global population, combined with the accelerating impacts of climate change and the rising CO_2 emissions, are leading to a growing demand for sustainable and green energy sources. As the world is trying to reduce the dependence on fossil fuels, a transition to a low carbon economy and the growth of new technologies to generate green energy are needed. In this context, green hydrogen could have a pivotal role for decarbonizing multiple sectors, including transportation, industry, and power generation [1].

Green hydrogen can be produced by electrolysis of water, an electrochemical process in which water is split by applying electrical energy,

* Corresponding author.
** Corresponding author. JARA – Fundamentals of Future Information Technology, Forschungszentrum Jülich, 52425, Jülich, Germany.
E-mail addresses: valentina.volanti@polito.it (V.M. Volanti), semenova@iwe.rwth-aachen.de (A. Semenova), andrea.zaffora@unipa.it (A. Zaffora), monica.santamaria@unipa.it (M. Santamaria), i.valov@fz-juelich.de (I. Valov).
[1] These authors contributed equally to this work.

https://doi.org/10.1016/j.matchemphys.2025.131713
Received 9 July 2025; Received in revised form 30 September 2025; Accepted 18 October 2025
Available online 19 October 2025

obtaining gaseous oxygen at the anode and gaseous hydrogen at the cathode, respectively. This process is considered completely green, and carbon neutral, when it is coupled with renewable electricity, produced for example by solar or wind sources. Furthermore, the versatility of hydrogen offers a path to get the global goals, since it could be used in various applications, from powering fuel cells in vehicles, to storing energy for grid stabilization [2,3].

Electrolysis principle itself is relatively simple, but it needs advanced technologies to achieve commercial viability at scale. Deployed water electrolysis technologies are alkaline water electrolyzers (AWEs) and proton exchange membrane water electrolyzers (PEMWEs). PEMWEs are efficient but they use electrocatalysts based on critical raw materials (CRMs) such as iridium at the anode, which is one of the rarest metal on Earth, and platinum at the cathode. AWEs work with a KOH-rich electrolyte, so they can operate without platinum-group metal (PGM) electrocatalysts but they suffer of electrodes stability issues, due to the very harsh environment at the anode, and low efficiency. However, this second process is more mature on an industrial point of view, and has been used in industrial settings for decades [4,5]. The overall efficiency of the device is also limited by the anodic oxygen evolution reaction (OER), which exhibits slower kinetics compared to the hydrogen evolution reaction (HER). This highlights the need for highly active and stable electrocatalytic materials. The benchmark material for OER is Ir oxide but it is CRM-based and expensive, limiting its large-scale application, being mostly used in acidic environment. In alkaline environment non-precious metal-based catalysts (NPMCs), particularly transition-metal compounds, have emerged as the most promising alternatives, due to their abundance, low-cost, and nontoxicity [6,7].

In this context, perovskites have been considered as significant candidates as electrocatalytic materials for OER, being a versatile class of materials with a specific crystal structure, and chemical formula ABO_3, where A is typically an alkaline earth metal, and B a transition metal. They have been widely studied for their remarkable catalytic activity, and tunable chemical compositions. By optimizing their composition and structure, it is possible to improve their stability and catalytic performances, making them an attractive solution for next-generation electrolysis systems [8,9]. Several compositions have been proposed to develop eligible catalysts for OER. Among these, $Ba_{0.5}Sr_{0.5}Co_{0.8}Fe_{0.2}O_{3-\delta}$ (BSCF) perovskite [10], is considered the state of the art perovskite material for OER performances because, thanks to the occupancy of the e_g orbitals, it can surpass the performances of RuO_2 and IrO_2 [11]. However, it faces serious stability issues, in fact it undergoes a phase transformation at relatively low temperatures, leading to the formation of new phases which present lower performances respect to the original compound [12].

Double perovskite $Pr_xBa_{1-x}CoO_{3-\delta}$ (PBCO) [13] exhibits good electrochemical performances in terms of overpotential and shows higher stability than BSCF, although its durability is not among the best reported for perovskites [14]. Indeed it has been demonstrated that, during the OER, the catalyst structure undergoes a transition to an amorphous state due to the chemical leaching of the A-site cation [12].

One of the state of art perovskite is $BaCo_{0.98}Ti_{0.02}O_{3-\delta}$:$Co_3O_4$ [15], in which starting from $BaCoO_3$ [16] perovskite, a cobalt excess Co_3O_4 is added, and it is doped with Ti, creating in that way a material that present high current densities for the OER, and a very stable behaviour compared to the previous examples, thanks to the reduction of oxygen vacancies into the crystal structure.

Other studies have explored perovskite activity toward the OER by means of DFT calculations, considering several compositions. These investigations demonstrated that $SrCoO_3$ (SCO) exhibits among the highest OER activities [17]. Therefore, several Sr-based perovskite oxides have been studied, like $La_{0.5}Sr_{0.5}CoO_3$ (LSCO), or $SrFeO_3$ (SFO) [18], presenting very good OER activity, thanks to the good adsorption and desorption capabilities of reaction intermediates. Anyway, $LaSrCoO_3$ and $BaSrCoO_3$ also face the problem of segregation and phase separation of Sr at high temperatures. This drawback can be mitigated by doping these perovskite materials with stable and high valent metal cations (V, Nb, Ti, Zr, Hf, Al) [15,19].

In this study, $SrCoO_{3-\delta}$ perovskites, in form of thin films, were studied as electrocatalytic materials for OER carried out in alkaline environment. SCO were synthesized by a chemical solution deposition method. The latter provides a highly controlled and reproducible thin films deposition, ensuring uniform composition, well-defined thickness, and excellent adhesion to the substrate. Working with thin films allowed to decouple extrinsic factors (e.g., binder effects, conductivity additives, random agglomeration) from the fundamental electrocatalytic properties of the active phase. The effect of the cobalt excess on the crystalline structure of $SrCoO_{3-\delta}$+Co_3O_4 and on the electrochemical performances was studied, as well as the effect of Ti doping to improve the long-term stability. Electrochemical measurements in aqueous solutions of 1 M KOH at 75 °C were used to assess the electrocatalytic activity and durability of the electrodes, in operating conditions close to the industrial ones. The durability of our electrodes was also assessed through an Accelerated Life Test (ALT), following the dynamic test protocol of EU technical report for testing of low temperature water electrolyzers, through a continuous cycling [20]. Findings highlight the potential of these highly active and durable electrodes for alkaline water electrolysis, free from platinum group metals (PGMs), and fabricated with a simple manufacturing process compared to methods usually employed for thin film production [21,22].

2. Materials and methods

2.1. Thin films synthesis

Chemical solution deposition method (CSD) has been used for thin film preparation [23]. A modified [12,13,15] propionic acid-based route [24] was applied for the deposition of $SrCoO_{3-\delta}$ (SCO) and $SrCoO_{3-\delta}$:Co_3O_4 (SCO:CB) materials. $Co(OOCCH_3)_2$, $Sr(OOCCH_3)_2$ were suspended in a mixture of propionic acid and propionic acid anhydride 1:5, removing the constitutional water of the acetate. Co_3O_4 admixture was realized by reducing Sr/Co ratio down to 0.75 in the precursor solution. To achieve different levels of Ti doping in the $SrCo_{1-x}Ti_xO_{3-\delta}$:$Co_3O_4$ (SCT:CB X), titanium (IV) oxide bis(2,4-pentanedionate) was added to the precursor solution. These solutions were adjusted to a final concentration of 0.3 M for the cobalt compound and refluxed for 1 h at 140 °C. Platinized Si (100) was used as a substrate, undergoing a preheating at 700 °C for 15 min to obtain textured film growth. Spin-coating was performed at 3000 rpm for 30 s, then pyrolyzed on a hotplate at 350 °C for 2 min. This coating and pyrolysis process was repeated 5 times, followed by a thermal treatment at 800 °C for 15 min in the air atmosphere. Samples with 1 at.%, 2 at.%, 3 at.%, 4 at.% and 5 at.% of Ti doping are named SCT:CB 1, SCT:CB 2, SCT:CB 3, SCT:CB 4 and SCT:CB 5, respectively.

2.2. Morphological characterization

2.2.1. Scanning electron microscopy

Samples' morphology was studied by using a FEI Quanta 200 Field Emission Gun Scanning Electron Microscope (FEG-SEM) coupled to EDX (X-ray Energy Dispersive system) to have information about the composition of the investigated thin films.

2.2.2. X-Ray Diffraction

Characterization of SCT:CB thin films was performed using Grazing Incidence X-Ray Diffraction (GIXRD) method to avoid substrate's contribution. Identification was done on Philips X'PERT diffractometer with Cu Kα radiation (40 kV, 40 mA). Data were obtained in 2θ range of 10°–65° with a step size of 0.02°.

2.2.3. XPS

To track the chemical state of the catalyst surface with degradation

an X-ray Photoelectron Spectroscopy (XPS) method was applied. The data were obtained with Phi 5000 VersaProbe II, ULVAC-Phi Inc. All spectras were corrected to C 1s signal with binding energy (BE) of 285 eV.

2.3. Electrochemical measurements

Electrochemical measurements were performed in a self-constructed and membrane-free electrochemical cell (see Fig. 1), designed for thin film electrodes, using a EC-Autolab 204 potentiostat (Metrohm), with a three-electrode configuration.

The electrolyte was an aqueous solution 1 M KOH, temperature was set at 75 °C, controlled by an automated thermostat, to emulate the operating conditions of a real electrolyzer. Prior to each measurement, the electrolyte was purged with N_2. The counter electrode was a gold plate, while the reference electrode was a Hg/HgO/1 M KOH. Reported electrode potentials, measured vs Hg/HgO, were then converted by referring to Reversible Hydrogen Electrode (RHE), following:

$$E_{RHE} = E_{Hg/HgO} + 0.1\ V + 0.059\ pH \quad (1)$$

To study electrocatalysts performances, in terms of Tafel slope and overpotential values, Linear Sweep Voltammetries, LSVs starting from 0.9 V RHE to 1.9 V RHE and EIS spectra at 1.72 V RHE (a.c. signal amplitude = 10 mV, frequency range: 0.1–10^5 Hz), were recorded. The impedance spectra were then modeled with ZSimpWin software with a suitable equivalent electric circuit to study the electrocatalytic activity of the electrodes. All the results were already corrected with a 95 % iR compensation. Tafel slope values were estimated with a steady state method. In particular, each value of potential was applied for about 10 min, until the steady state value of current was reached.

Electrocatalysts durability was assessed by an ALT, conducted by continuously cycling the sample at a scan rate of 100 mV s^{-1} between 1 V and 2 V RHE.

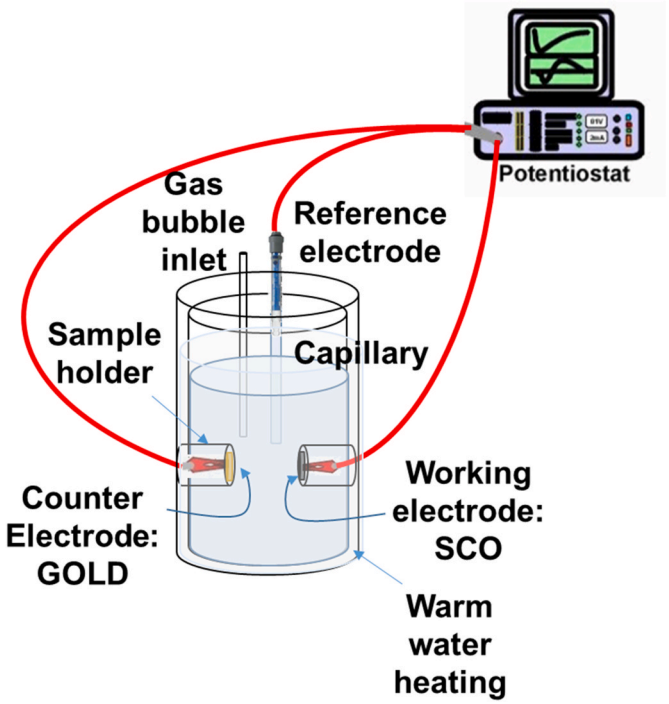

Fig. 1. Cell configuration used for electrochemical measurements.

3. Results and discussion

3.1. Morphological characterization

Fig. 2a) shows SEM micrograph related to platinized Si substrate whilst SEM image related to SCO sample is reported in Fig. 2b).

As it is possible to note, no particular features are present before and after the deposition of perovskite thin films by CSD method. Surface roughness was assessed to be between 1 and 10 nm in previous works [12,13,15]. It is noteworthy to mention that surface morphology did not change by changing deposition conditions, both adding Co excess (i.e. SCO:CB sample) and by Ti doping (i.e. SCT:CB samples).

Fig. 2c shows x-ray diffractograms related to SCO:CB sample and all SCT:CB samples, varying Ti doping between 1 at.% and 5 at.%., whilst view on the SCO:CB structure along the [210] direction is shown Fig. 2d). All the samples were identified as 6R structure in trigonal symmetry ($R\bar{3}$, Nr. 148) reported by Sun et al. (ICSD N° 81312) [25]. $Co^{3+/4+}$ ions form CoO_6 chains oriented along [001] direction, being separated by trigonal prisms. Main diffraction peaks can be found at 2θ = 18.67°, 28.63°, 32.64°, 43.82°, 55.69°. SCT:CB lattice parameters change from a = 9.49 Å and c = 12.41 Å for 0 % Ti-doping to a = 9.49 Å and c = 12.49 Å for 2 % Ti-doped samples. At 3 % Ti-doping the formation of additional planes is observed, which is assumed to be related to a new polymorph, with a decreased *c*-parameter (*c* = 12.41 Å) and the presence of two new peaks at 2θ = 31.3° and 38.6° (although their intensity appears reduced due to the scaling of the graph). However, due to a low crystallinity, we are unable to accurately interpret this polymorph. 2 % of Ti is the limit concentration up to which the 6R structure is preserved, and a low crystallinity at 2 % is observed due to the lattice strains caused by ionic radius (Ti^{4+} vs $Co^{3+/4+}$) mismatch; with 3 % and above of Ti^{4+}, the lattice relaxation results into a new phase formation. All the samples presented contain Co_3O_4 (ICSD N° 27497) collateral phase, indeed it is possible to recognize the characteristic peaks at 2θ = 36.97° and 44.96°.

3.2. Electrochemical characterization

Electrochemical measurements were carried out to evaluate the electrocatalytic behavior of synthesized perovskites, by recording LSVs and impedance spectra. LSVs recorded at a scan rate of 10 mV s^{-1} are reported in Fig. 3a), considering a 95 % iR drop correction.

To evaluate OER activity of investigated perovskite thin films, we estimated the onset overpotential, η_{onset}, defined as the overpotential value obtained when the current density reaches 1 mA cm^{-2}, and the overpotential at 10 mA cm^{-2}, η_{10}. These values are reported in Table 1 for all the samples.

As it is possible to notice, B-type substitution, i.e. the excess of cobalt (SCO:CB sample), improves the electrocatalytic activity of SCO sample showing both a reduction of η_{onset} and η_{10} values, 284 mV and 343 mV respectively for SCO:CB sample, and 298 mV and 357 mV respectively for SCO sample. This result is in accordance with the data reported in literature for BCO perovskite system, where authors reported improved electrocatalytic performances but worse long-time stability behaviour [15]. Indeed, the excess of cobalt could lead to the formation of extra active sites and, at the same time, can influence oxygen stoichiometry, by increasing the number of oxygen vacancies, which enhances conductivity, diffusion and oxygen release [9]. These effects could be in contrast, taking into account the peculiar reaction mechanism for OER on perovskite materials. It is commonly accepted that OER on perovskite can occur through two different mechanisms: the conventional mechanism, or Adsorbate Evolution Mechanism (AEM), and the Lattice Oxygen oxidation Mechanism (LOM) [26,27]. In the AEM mechanism, O_2 formation occurs through the adsorption of intermediate species (OH*, O*, OOH*) on the catalyst surface. In the case of LOM mechanism, the lattice oxygen of the perovskite actively participates in the reaction, leading to

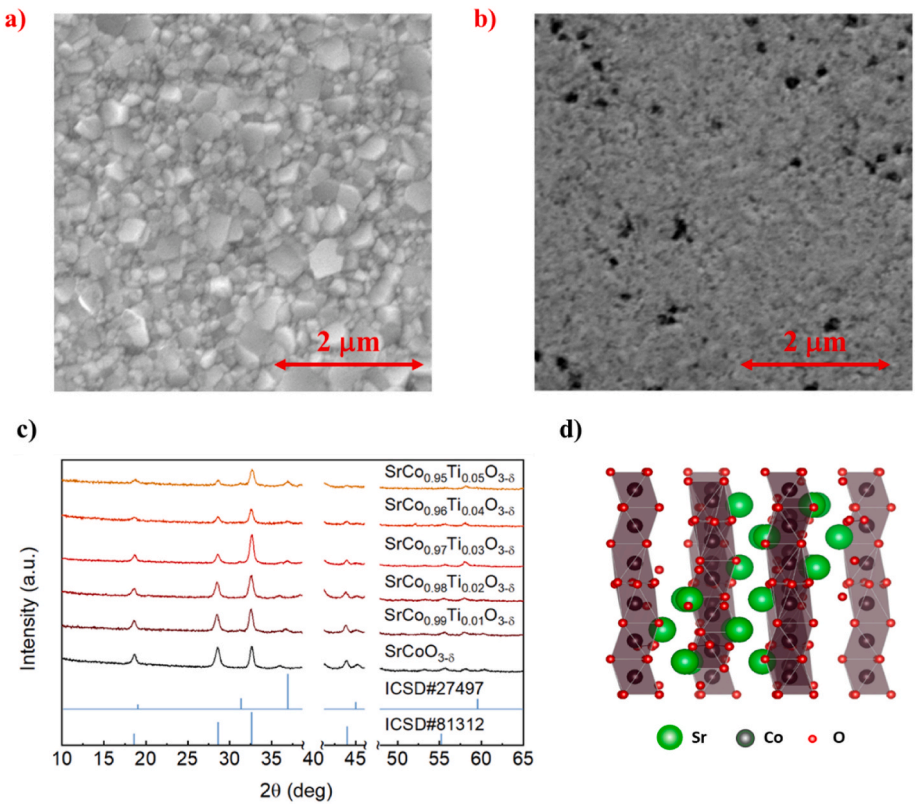

Fig. 2. a), SEM micrograph related to platinized Si substrate (magnification: 20000x) and b) SEM image related to SCO sample (magnification: 20000x). c) GIXRD patterns of the SCO, SCO:CB and SCT:CB samples and d) view on the SCO:CB structure along the [210] direction.

the consequent formation of oxygen vacancies and the recombination of hydroxyl species to generate O_2. This second process is favored by an high mobility of lattice oxygen and a low energy vacancy formation [9]. For $SrCoO_{3-\delta}$ perovskite, the dominant OER mechanism is usually considered the LOM, thanks to its electronics band structure, and the presence of a high number of oxygen vacancies, which enhance oxygen mobility within the structure [28]. When the material is subjected to anodic potentials during OER, lattice oxygen can be directly oxidized, rather than following the conventional pathway with adsorbed intermediate. On the other hand, a high vacancy concentration can also lead to Sr ions diffusing out of the lattice. A strategy to mitigate this issue can be, for instance, the Ti doping [19]. In fact, Ti presence could lead to a change in oxidation level of Co species in SCO structure, namely Co^{2+} and Co^{3+} that are replaced by Ti^{4+} species. This process can be expressed according to Kröger-Vink notation as:

$$2Co_{Co}^{x} + V_{O}^{\cdot\cdot}(SrCoO_{3-\delta}) \xrightarrow{2TiO_2} 2Ti_{Co}^{\cdot} + O_{O}^{x} + Co_2O_3 \quad (2)$$

resulting in a decrease in oxygen vacancies concentration. Moreover, as reported in literature, Ti^{4+} substitution at the B-site has been shown to reduce oxygen deficiency by forming strong Ti–O bonds and thus suppressing the formation of oxygen vacancies [29,30].This can cause a decrease in overall perovskite conductivity due to the reduction of oxygen possible pathways but, at the same time, it could help in limiting degradation phenomena of the crystalline structure (see below) and the possibility to have evolution of lattice oxygen from the crystal [31].

Averagely, the presence of Ti doping led to worse electrochemical performance than SCO:CB, both in terms of η_{onset} and η_{10} values. In fact, lowest onset potential was registered with SCT:CB 5 sample (i.e. 1.533 V RHE meaning 303 mV as overpotential) whilst the highest one was recorded by using SCT:CB 4 sample (i.e. 1.566 V RHE meaning 336 mV as overpotential). Anyway, these onset potential values are comparable to those recorded for PBCO samples and are lower with respect to BSCF samples, whose onset potential is about 1.6 V RHE [12].

Between 1 and 3 % of Ti doping the electrocatalytic behaviour is similar, estimating η_{10} values between 372 and 379 mV, whilst with 4 % of Ti doping in SCO:CB sample there is a worsening in the activity of the catalyst, reaching 10 mA cm^{-2} with an overpotential of 402 mV. A further increase in Ti doping, i.e. 5 %, led to an improvement in electrochemical performances (i.e. η_{10} = 362 mV), even if this result is not highly reproducible, since performances decreased by repeating electrochemical measurements. This behaviour has been already observed with high level of Ti doping in a BCT:CB system [15]. Therefore, although a reduction in the catalytic activity of our sample has been observed, the simultaneous presence of Co excess and Ti doping may help achieve a balance between activity and stability of our material. Comparing η_{onset} and η_{10} values obtained by using $SrCoO_{3-\delta}$ and $SrCo_{1-x}Ti_xO_{3-x}$ perovskites with those reported in literature, it is worth noting that SCO:CB sample outperformed many of the perovskites materials, and obtained with both A-site and B-site doping [32,33], considering that samples studied in this work had no binder, as typically used in literature for improving electrochemical performances.

Tafel plots (overpotential η vs. log(i)) are shown in Fig. 3b). These plots were obtained by taking into account the current density value recorded by applying electrode potential values until a steady state current density value was reached.

The linear portion of the Tafel plot can be matched with the given equation:

$$\eta = a + b \cdot log(i) \quad (3)$$

where a is directly proportional to the logarithm of the exchange current density, meaning that a quantifies intrinsic electrocatalytic properties of the material and b is known as the slope of the Tafel line. Other than its relationship with electrocatalytic activity of the material, since a lower b value means a lower overpotential to increase of a decade the current density value, Tafel slope value can be related to the reaction mechanism. Given a reaction and assumed a reaction mechanism, b can be

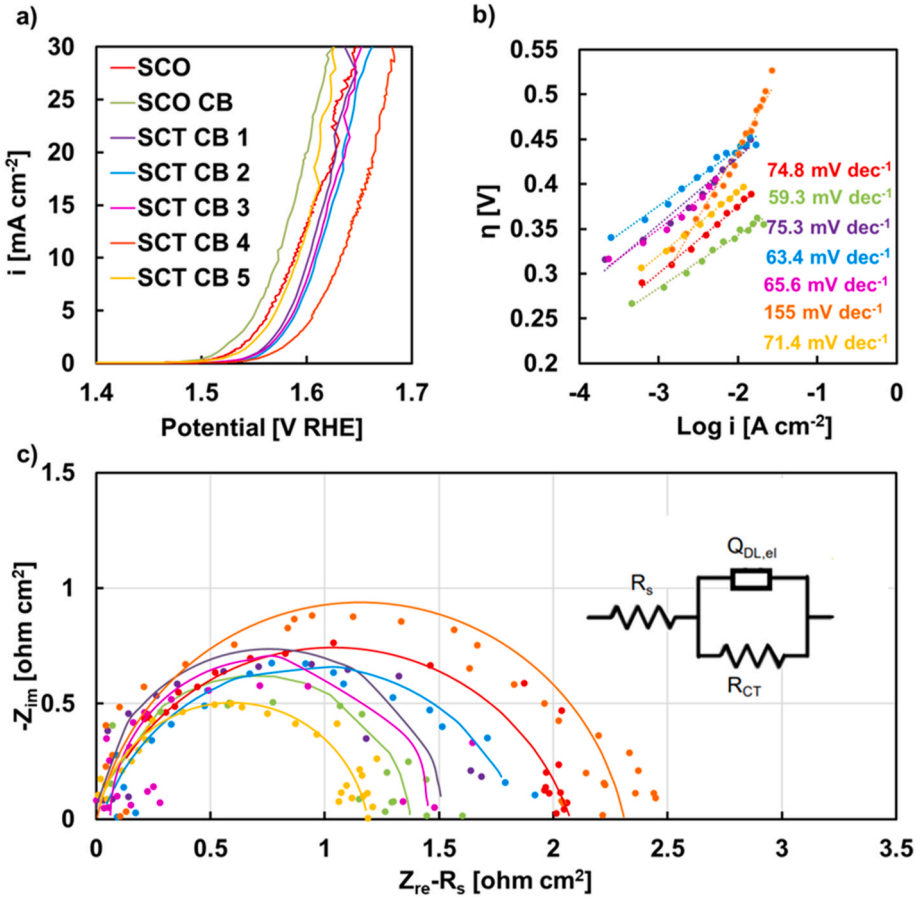

Fig. 3. a) Current density vs. potential curves, b) Steady State Tafel plots and c) Electrochemical impedance spectra recorded at 0.8 V Hg/HgO (1.72 V RHE) for all the investigated electrodes. Inset: equivalent electrical circuit used for spectra fitting procedure. Continuous lines: fitting data.

Table 1
η_{onset} and η_{10} values estimated from LSV reported in Fig. 3a).

Sample	η_{onset} [mV]	η_{10} [mV]
SCO	298	357
SCO:CB	284	343
SCT:CB 1	322	372
SCT:CB 2	327	379
SCT:CB 3	323	376
SCT:CB 4	336	402
SCT:CB 5	303	362

directly related to the rate determining step. The value of Tafel slope from SCO to 3 % of doping is between 60 mV dec^{-1} and 70 mV dec^{-1}, in the usual range for OER with perovskite [14]. SCT:CB sample with 4 % of Ti doping presents a very high value of Tafel slope, in agreement with the lowest recorded electrocatalytic performance. Notably, Tafel slope values are comparable with data reported for perovskites used for OER [32,33].

EIS was performed at 0.8 V Hg/HgO (i.e. 1.72 V RHE), and Nyquist plots related to all the investigated samples are reported in Fig. 3c). Electrochemical behaviour of all electrodes was modeled by considering the equivalent electric circuit (EEC) shown in the inset of Fig. 3c). EEC involves only one time constant, i.e. a series between R_s, that is the resistance of the electrolyte, and a parallel between R_{CT}, the charge transfer resistance, and $Q_{DL,el}$, the constant phase element (CPE) used for modelling the non-ideal electric double layer capacitance of the electrode. Low R_{CT} values indicate better electrocatalytic performances, therefore it is possible to compare electrochemical performances by looking at these values. Fitting parameters of EIS spectra are reported in

Table 2
Fitting parameters of EIS spectra recorded at 0.8 V Hg/HgO (i.e. 1.72 V RHE) (see Fig. 3c)). $R_s = 7\ \Omega\ cm^2$.

Sample	R_{CT} [$\Omega\ cm^2$]	$Q_{DL,el}$ [$S\ s^n\ cm^{-2}$]	n	χ^2
SCO	2.1	2.8×10^{-3}	0.79	2.5×10^{-4}
SCO:CB	1.3	2.7×10^{-4}	0.94	3.5×10^{-4}
SCT:CB 1	1.5	1.2×10^{-3}	0.98	3.4×10^{-4}
SCT:CB 2	1.8	2.5×10^{-3}	0.79	3.1×10^{-4}
SCT:CB 3	1.4	9.1×10^{-4}	0.99	3.9×10^{-4}
SCT:CB 4	2.3	1.2×10^{-3}	0.86	3.8×10^{-4}
SCT:CB 5	1.2	2.3×10^{-3}	0.89	2.7×10^{-5}

Table 2. Lowest R_{CT} values were found for SCO:CB and SCT:CB 5 samples, i.e. 1.3 and 1.2 $\Omega\ cm^2$, respectively, in agreement with LSVs shown in Fig. 3a). Highest R_{CT} values were found for SCO and SCT:CB 4 samples, almost twice with respect to those found for best samples, whilst similar R_{CT} values were estimated for the other investigated samples.

Using SCO:CB sample, the lowest values of Tafel slope and R_{CT} were estimated, consistently with a predominant contribution of LOM mechanism [34]. Ti doping led to worse performances, as evidenced by an increase of Tafel slope and R_{CT} values. However, up to the 3 % of doping, these values remain relatively constant and comparable to results reported using perovskites for OER [27].

To investigate the electrochemical stability of the electrocatalytic materials, an ALT was carried out by continuously cycling the sample [35–38] at a scan rate of 100 mV s^{-1} within the potential range 1–2 V RHE. Stability test for all the investigated samples is reported in Fig. 4 where current density value recorded at 2 V RHE for each cycle is reported. The drop in current density value was considered as the end of

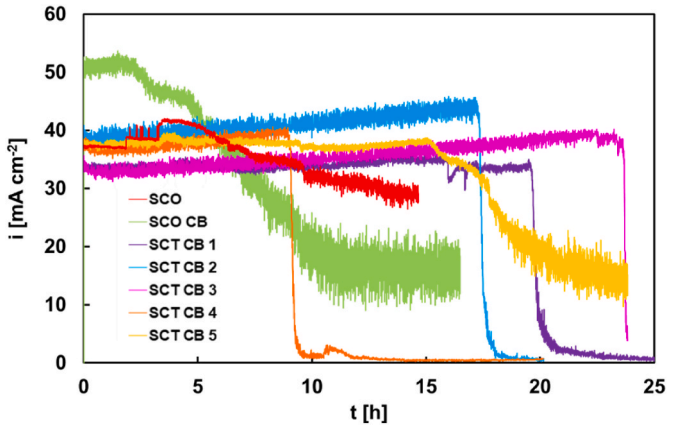

Fig. 4. ALT related to all the investigated electrodes using the current density j at 2 V RHE during CV sweeps at 100 mV s^{-1} and 75 °C in 1 M KOH.

the test due to the complete degradation of the electrocatalytic layer.

As noted from LSV, SCO:CB demonstrated the best electrocatalytic initial performance, showing the highest current density value at the beginning of the stability test. It is worth noting that SCO:CB is also the sample with the lowest stability, demonstrating that Ti doping improved electrocatalyst lifetime, regardless on the specific thin film composition. In particular, SCT:CB 3 sample showed the best stability performance, reaching 24 h before the complete failure, related to the complete leaching of the thin film. Comparing the durability of our samples to some of the best perovskite OER catalysts reported in the literature (i.e. PBCO and BSCF [15]) it is noteworthy to mention that SCT:CB perovskites demonstrated greater stability and retain its electrocatalytic performances for a longer time. In fact, although BSCF initially achieves higher current density, i.e. 68 mA cm^2, its performance decreases quite rapidly after only 200–300 cycles. PBCO samples, on the other hand, maintains a current density of about 48 mA cm^2 for about 11 h, i.e. a similar stability performance with respect to that assessed for SCT:CB 4 sample, that is the worst sample. As it was mentioned in previous section, the replacement of Co with Ti ion, reduces the formation of oxygen vacancies, limiting the mobility of Sr inside the framework [31].

3.3. XPS characterization

To track the surface chemical changes in initial structure of SCT:CB under operation, XPS data were collected within Sr 3d, Co $2p_{3/2}$ and Ti 2p regions (see Fig. 5). Samples' composition, related to most performing sample, i.e. SCO:CB, and Ti-doped samples, up to 3 % of doping (most stable sample), obtained by XPS measurements are reported in Table 3.

Related to samples composition reported in Tables 3 and it is important to mention that Pt presence is only related to the substrate (i.e. platinized Si). Regarding Sr 3d core levels, four distinct peaks can be observed (see Fig. 5a) indicating doublets for both the Sr $3d_{3/2}$ (BE = 134.0 eV and 135.8 eV) and Sr $3d_{5/2}$ (BE = 132.9 eV and 134.6 eV) levels, which correspond to Sr^{2+} state [39]. Moreover, based on what reported in literature, it is possible to assign the peak at lower binding energy to Sr within the lattice ($Sr_{lattice}$) and the peak to higher binding energy to Sr on the surface ($Sr_{surface}$) [40]. After Ti doping (see Fig. 5b and c), an increase of $Sr_{lattice}$ contribution can be observed, suggesting a more difficult Sr leaching from the lattice. Electrochemical cycling, i.e. aging process, led to a single doublet in XPS spectrum (see Fig. 5a–c)) remaining with Sr $3d_{5/2}$ peak positioned between 133.5 eV and 133.1 eV and Sr $3d_{3/2}$ peak positioned between 135.2 eV and 134.8 eV, depending on Ti doping level, therefore with a higher BE with respect to as-formed samples.

Surface cobalt ions are presented as the mixture of Co^{2+}/Co^{3+} oxidation states, referred to the data of Co_3O_4 (BE = 779.6 eV [41]) and $ZnCo_2O_4$ (BE = 780.4 eV [42]). Indeed, it is possible to estimate Co^{3+}/Co^{2+} ratio by taking into account at.% of Co_3O_4 and Co^{3+} species, derived from Co $2p_{3/2}$ XPS spectrum fitting. Considering that Co_3O_4 spinel structure is composed by CoO (i.e. Co^{2+}) and Co_2O_3 (i.e. Co^{3+}) with tetrahedral and octahedral geometrical sites, respectively, in a ratio 1:2 [29,43], Co^{3+}/Co^{2+} ratio can be easily calculated. In particular, SCO:CB sample presented the highest Co^{3+}/Co^{2+} ratio before cycling, i.e. 3.11, whilst, for Ti-doped samples, Co^{3+}/Co^{2+} ratio was about 2. This aspect results particularly relevant because Co^{3+} species can be seen as the precursor state that can be further oxidized under anodic potentials to form electrocatalytically active Co^{4+} species. In this regard, the excess of Co^{3+} with respect to Co^{2+} species in SCO:CB sample provides a larger amount of species that can undergo the Co^{3+}/Co^{4+} transition during OER. Indeed, the lowest overpotential observed for SCO:CB sample can be rationalized by taking into account its higher initial Co^{3+} content, which enhances the ability of the material to reach and sustain the Co^{3+}/Co^{4+} redox equilibrium under reaction conditions.

As mentioned, Ti doping causes partial reduction of Co^{3+} ions with a BE shift (upon doping with 2 % Ti) [44], identifying all the dopant ions as Ti^{4+} species (BE = 458.2 eV for TiO_2 [45]) having a splitting energy Δ = 5.7 eV.

After cycling, for all the Ti doping levels, ratio between Co^{3+}/Co^{2+} surface species increases, from 2 to 6.76 for SCT:CB 1 sample and from 2 to 2.2 for 3 % Ti-doping, indicating cations with higher oxidation state to be responsible for the stability and being in agreement with studies reported [46]. Ti surface species keep initial splitting energy and shift towards higher binding energies, indicating change in the ion's coordination. Splitting into two doublets is suggested to indicate an agglomeration of remaining Ti species in the vicinity of leached Sr cations. Moreover, Sr/Co ratio increases by increasing Ti doping content, from 0.056 for SCO:CB sample to 0.079 for SCT:CB 3 sample, demonstrating that electrochemical stability of SCT:CB 3 sample can be related to higher Sr content during cycling and confirming the role of a dopant Ti^{4+} with the highest oxidation state as a stabilizer of *A*-sites in perovskites [15].

4. Conclusions

$SrCoO_{3-\delta}$ and $SrCo_{1-x}Ti_xO_{3-\delta}$ perovskites thin films were successfully deposited by chemical bath deposition method to be used as electrocatalytic layers for OER carried out during water electrolysis in alkaline environments. $SrCoO_{3-\delta}$ perovskites thin films were prepared inducing an excess of Co in the perovskite structure, and by doping with Ti in order to induce a substitution in *B*-site of perovskite.

All the investigated perovskites can be used as electrocatalytic layers for OER, but sample with Co excess (i.e. SCO:CB) demonstrated the best electrochemical performance, in terms of η_{onset} and R_{CT} values (284 mV and 1.3 Ω cm^2, respectively), assessing a Tafel slope of 59 mV dec^{-1}, measured in 1 M KOH aqueous solution at 75 °C. Ti-doping did not have a direct beneficial effect on electrocatalytic activity but Ti-doped perovskites had a higher durability with respect to base $SrCoO_{3-\delta}$ perovskite and SCO:CB sample. In fact, SCT:CB 3 sample showed a 24 h stable electrochemical performance, compared to a 10 h stable performance of SCO:CB sample. Moreover, it was assessed that the main degradation mechanism was surface Sr leaching and Ti-doping was effective in reducing it, confirming the role of a dopant Ti^{4+} as a stabilizer of *A*-sites in $SrCoO_{3-\delta}$ perovskites.

CRediT authorship contribution statement

Valentina Maria Volanti: Writing – review & editing, Writing – original draft, Investigation, Formal analysis, Data curation. **Anastasiia Semenova:** Writing – review & editing, Writing – original draft, Investigation, Formal analysis, Data curation. **Andrea Zaffora:** Writing – review & editing, Visualization, Supervision, Methodology, Formal analysis, Data curation. **Monica Santamaria:** Writing – review &

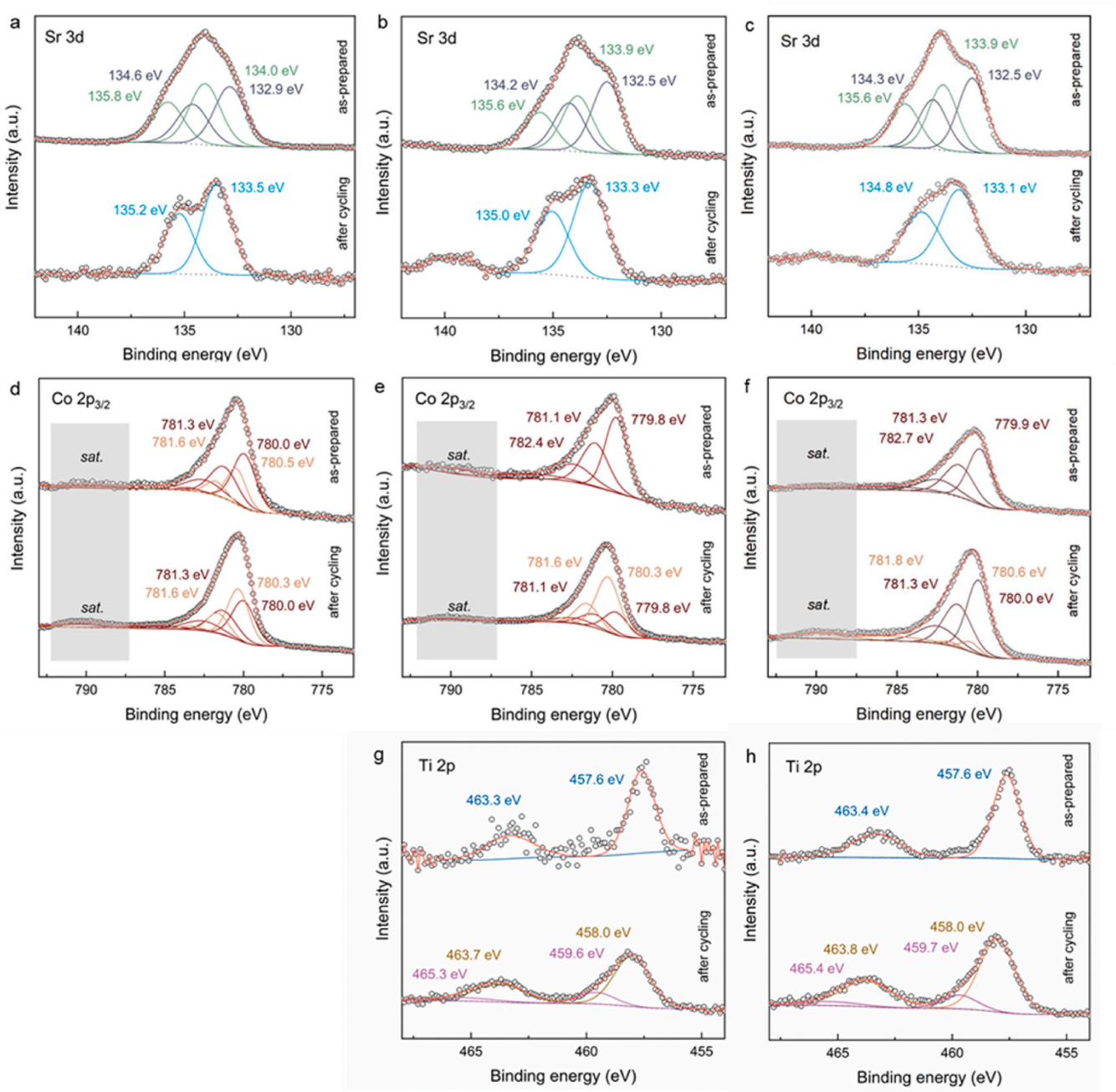

Fig. 5. Sr 3d and Co $2p_{3/2}$ and Ti 2p XPS fitted spectra on as-prepared and after 100 CV cycles in 1 M KOH for SCO:CB (a, d), SCT:CB 1 (b, e, g), SCT:CB 3 (c, f, h).

Table 3
Samples composition estimated through XPS measurements.

Sample	C 1s [at. %]	O 1s [at. %]	Ti 2p [at.%]	Co $2p_{3/2}$ [at.%]	Sr 3d [at.%]	Pt 4f [at.%]
SCO:CB	22.2	59	–	3.3	12.4	3.1
SCT:CB 1	24.3	58.2	0.2	6.6	9.5	1.2
SCT:CB 2	21	58.8	0.4	8.3	8.8	2.6
SCT:CB 3	23	58	0.6	5.9	10	2.6

editing, Visualization, Supervision, Resources, Methodology. **Ilia Valov:** Writing – review & editing, Visualization, Supervision, Resources, Methodology, Conceptualization.

Declaration of competing interest

The authors declare that they have no known competing financial interests or personal relationships that could have appeared to influence the work reported in this paper.

Acknowledgements

We thank Dr. Heinrich Hartmann and Dr. Astrid Besmehn (ZEA-3, Forschungszentrum Jülich) for conducting XPS measurements.

Data availability

Data will be made available on request.

References

[1] A.I. Osman, N. Mehta, A.M. Elgarahy, M. Hefny, A. Al-Hinai, A.H. Al-Muhtaseb, D. W. Rooney, Hydrogen Production, Storage, Utilisation and Environmental Impacts: a Review, Springer International Publishing, 2022, https://doi.org/10.1007/s10311-021-01322-8.

[2] IRENA, Green Hydrogen Cost Reduction: Scaling up Electrolysers to Meet the 1.5 °C Climate Goal, 2020. Abu Dhabi.

[3] J.A. Luque-Urrutia, T. Ortiz-García, M. Solà, A. Poater, Green energy by hydrogen production from water splitting, water oxidation catalysis and acceptorless dehydrogenative coupling, Inorganics 11 (2023), https://doi.org/10.3390/inorganics11020088.

[4] C. Santoro, A. Lavacchi, P. Mustarelli, V. Di Noto, L. Elbaz, D.R. Dekel, F. Jaouen, What is next in anion-exchange membrane water electrolyzers? Bottlenecks, benefits, and future, ChemSusChem 15 (2022), https://doi.org/10.1002/cssc.202200027.

[5] S.A. Grigoriev, V.N. Fateev, D.G. Bessarabov, P. Millet, Current status, research trends, and challenges in water electrolysis science and technology, Int. J. Hydrogen Energy 45 (2020) 26036–26058, https://doi.org/10.1016/j.ijhydene.2020.03.109.

[6] D. Zhou, P. Li, W. Xu, S. Jawaid, J. Mohammed-Ibrahim, W. Liu, Y. Kuang, X. Sun, Recent advances in non-precious metal-based electrodes for alkaline water electrolysis, ChemNanoMat 6 (2020) 336–355, https://doi.org/10.1002/cnma.202000010.

[7] X. Xie, L. Du, L. Yan, S. Park, Y. Qiu, J. Sokolowski, W. Wang, Y. Shao, Oxygen evolution reaction in alkaline environment: material challenges and solutions, Adv. Funct. Mater. 32 (2022), https://doi.org/10.1002/adfm.202110036.

[8] W.T. Hong, M. Risch, K.A. Stoerzinger, A. Grimaud, J. Suntivich, Y. Shao-Horn, Toward the rational design of non-precious transition metal oxides for oxygen electrocatalysis, Energy Environ. Sci. 8 (2015) 1404–1427, https://doi.org/10.1039/c4ee03869j.

[9] L.B. Liu, C. Yi, H.C. Mi, S.L. Zhang, X.Z. Fu, J.L. Luo, S. Liu, Perovskite Oxides Toward Oxygen Evolution Reaction: Intellectual Design Strategies, Properties and Perspectives, Springer Nature Singapore, 2024, https://doi.org/10.1007/s41918-023-00209-2.

[10] J. Suntivich, K.J. May, H.A. Gasteiger, J.B. Goodenough, Y. Shao-Horn, A perovskite oxide optimized for oxygen evolution catalysis from molecular orbital principles, Science 334 (2011) 1383–1385, https://doi.org/10.1126/science.1212858.

[11] Y. Lee, J. Suntivich, K.J. May, E.E. Perry, Y. Shao-Horn, Synthesis and activities of rutile IrO 2 and RuO 2 nanoparticles for oxygen evolution in acid and alkaline solutions, J. Phys. Chem. Lett. 3 (2012) 399–404, https://doi.org/10.1021/jz2016507.

[12] D.S. Bick, A. Kindsmüller, G. Staikov, F. Gunkel, D. Müller, T. Schneller, R. Waser, I. Valov, Stability and degradation of perovskite electrocatalysts for oxygen evolution reaction, Electrochim. Acta 218 (2016) 156–162, https://doi.org/10.1016/j.electacta.2016.09.116.

[13] D.S. Bick, J.D. Griesche, T. Schneller, G. Staikov, R. Waser, I. Valov, Pr x Ba 1-x CoO 3 oxide electrodes for oxygen evolution reaction in alkaline solutions by chemical solution deposition, J. Electrochem. Soc. 163 (2016) F166–F170, https://doi.org/10.1149/2.0311603jes.

[14] R. Khan, M.T. Mehran, S.R. Naqvi, A.H. Khoja, K. Mahmood, F. Shahzad, S. Hussain, Role of perovskites as a bi-functional catalyst for electrochemical water splitting: a review, Int. J. Energy Res. 44 (2020) 9714–9747, https://doi.org/10.1002/er.5635.

[15] D.S. Bick, A. Kindsmüller, D.-Y. Cho, A.Y. Mohamed, T. Bredow, H. Laufen, F. Gunkel, D.N. Mueller, T. Schneller, R. Waser, I. Valov, Self-assembling oxide catalyst for electrochemical water splitting, ArXiv (2017), https://doi.org/10.48550/arXiv.1707.03346.

[16] T. Tabari, M. Kobielusz, D. Singh, J. Yu, W. Macyk, Cobalt-/Copper-Containing perovskites in oxygen evolution and reduction reactions, ACS Appl. Eng. Mater. 1 (2023) 2207–2216, https://doi.org/10.1021/acsaenm.3c00288.

[17] I.C. Man, H.Y. Su, F. Calle-Vallejo, H.A. Hansen, J.I. Martínez, N.G. Inoglu, J. Kitchin, T.F. Jaramillo, J.K. Nørskov, J. Rossmeisl, Universality in oxygen evolution electrocatalysis on oxide surfaces, ChemCatChem 3 (2011) 1159–1165, https://doi.org/10.1002/cctc.201000397.

[18] S. Yagi, I. Yamada, H. Tsukasaki, A. Seno, M. Murakami, H. Fujii, H. Chen, N. Umezawa, H. Abe, N. Nishiyama, S. Mori, Covalency-reinforced oxygen evolution reaction catalyst, Nat. Commun. 6 (2015) 1–6, https://doi.org/10.1038/ncomms9249.

[19] N. Tsvetkov, Q. Lu, L. Sun, E.J. Crumlin, B. Yildiz, Improved chemical and electrochemical stability of perovskite oxides with less reducible cations at the surface, Nat. Mater. 15 (2016) 1010–1016, https://doi.org/10.1038/nmat4659.

[20] Georgios Tsotridis, A. Pilenga, Eu H2 protocols. https://doi.org/10.2760/58880., 2021.

[21] Z. Chen, P. He, D. Wu, C. Chen, M. Mujahid, Y. Li, Y. Duan, Processing and preparation method for high-quality opto-electronic perovskite film, Front. Mater. 8 (2021) 1–13, https://doi.org/10.3389/fmats.2021.723169.

[22] H. Wang, M. Zhou, P. Choudhury, H. Luo, Perovskite oxides as bifunctional oxygen electrocatalysts for oxygen evolution/reduction reactions – a mini review, Appl. Mater. Today 16 (2019) 56–71, https://doi.org/10.1016/j.apmt.2019.05.004.

[23] J.E. ten Elshof, Chemical solution deposition of oxide thin films. https://doi.org/10.1016/B978-0-08-102945-9.00012-5, 2022.

[24] U. Hasenkox, C. Mitze, R. Waser, Metal propionate synthesis of magnetoresistive La1-x(Ca,Sr)xMnO3 thin films, J. Am. Ceram. Soc. 80 (1997) 2709–2713, https://doi.org/10.1111/j.1151-2916.1997.tb03180.x.

[25] J. Sun, G. Li, Z. Li, L. You, J. Lin, Crystal growth and structure determination of oxygen-deficient Sr 6Co5O15, Inorg. Chem. 45 (2006) 8394–8402, https://doi.org/10.1021/ic060862m.

[26] B.J. Kim, E. Fabbri, M. Borlaf, D.F. Abbott, I.E. Castelli, M. Nachtegaal, T. Graule, T.J. Schmidt, Oxygen evolution reaction activity and underlying mechanism of perovskite electrocatalysts at different pH, Mater. Adv. 2 (2021) 345–355, https://doi.org/10.1039/d0ma00661k.

[27] L. Lu, M. Sun, T. Wu, Q. Lu, B. Chen, C. Hei Chan, H. Ho Wong, Z. Li, B. Huang, Perovskite oxides for electrocatalytic Hydrogen/Oxygen evolution reaction, Chemelectrochem (2025), https://doi.org/10.1002/celc.202400648, 202400648.

[28] J. Song, C. Wei, Z.F. Huang, C. Liu, L. Zeng, X. Wang, Z.J. Xu, A review on fundamentals for designing oxygen evolution electrocatalysts, Chem. Soc. Rev. 49 (2020) 2196–2214, https://doi.org/10.1039/c9cs00607a.

[29] M.G. Ahmed, Y.F. Tay, M. Zhang, S.Y. Chiam, L.H. Wong, Tailoring surface electronic structure of spinel Co3O4 oxide via Fe and Cu substitution for enhanced oxygen evolution reaction, ACS Mater. Lett. 6 (2024) 4756–4764, https://doi.org/10.1021/acsmaterialslett.4c00857.

[30] C. Su, W. Wang, Y. Chen, G. Yang, X. Xu, M.O. Tadé, Z. Shao, SrCo 0.9 Ti 0.1 O 3−δ as a new electrocatalyst for the oxygen evolution reaction in alkaline electrolyte with stable performance, ACS Appl. Mater. Interfaces 7 (2015) 17663–17670, https://doi.org/10.1021/acsami.5b02810.

[31] H.A. Tahini, X. Tan, U. Schwingenschlögl, S.C. Smith, Formation and migration of oxygen vacancies in SrCoO3 and their effect on oxygen evolution reactions, ACS Catal. 6 (2016) 5565–5570, https://doi.org/10.1021/acscatal.6b00937.

[32] X. Sun, Y. Yuan, S. Liu, H. Zhao, S. Yao, Y. Sun, M. Zhang, Y. Liu, Z. Lin, Recent advances in Perovskite oxides for oxygen evolution reaction: structures, mechanisms, and strategies for performance enhancement, Adv. Funct. Mater. 35 (2025) 1–27, https://doi.org/10.1002/adfm.202416705.

[33] L. Lu, M. Sun, T. Wu, Q. Lu, B. Chen, C. Hei Chan, H. Ho Wong, Z. Li, B. Huang, Perovskite oxides for electrocatalytic Hydrogen/Oxygen evolution reaction, Chemelectrochem 12 (2025), https://doi.org/10.1002/celc.202400648.

[34] Y. Pan, X. Xu, Y. Zhong, L. Ge, Y. Chen, J.P.M. Veder, D. Guan, R. O'Hayre, M. Li, G. Wang, H. Wang, W. Zhou, Z. Shao, Direct evidence of boosted oxygen evolution over perovskite by enhanced lattice oxygen participation, Nat. Commun. 11 (2020) 1–10, https://doi.org/10.1038/s41467-020-15873-x.

[35] M.R. Gao, Y.F. Xu, J. Jiang, Y.R. Zheng, S.H. Yu, Water oxidation electrocatalyzed by an efficient Mn3O 4/CoSe2 nanocomposite, J. Am. Chem. Soc. 134 (2012) 2930–2933, https://doi.org/10.1021/ja211526y.

[36] M. Ledendecker, S. Krick Calderón, C. Papp, H. Steinrück, M. Antonietti, M. Shalom, The synthesis of nanostructured Ni 5 P 4 films and their use as a non-noble bifunctional electrocatalyst for full water splitting, Angew. Chemie Int. Ed. 54 (2015) 12361–12365, https://doi.org/10.1002/anie.201502438.

[37] J.W.D. Ng, M. Tang, T.F. Jaramillo, A carbon-free, precious-metal-free, high-performance O2 electrode for regenerative fuel cells and metal-air batteries, Energy Environ. Sci. 7 (2014) 2017–2024, https://doi.org/10.1039/c3ee44059a.

[38] F. Paquin, J. Rivnay, A. Salleo, N. Stingelin, C. Silva, Multi-phase semicrystalline microstructures drive exciton dissociation in neat plastic semiconductors, J. Mater. Chem. C 3 (2015) 10715–10722, https://doi.org/10.1039/b000000x.

[39] H. Van Doveren, J.A.T.H. Verhoeven, XPS spectra of Ca, Sr, Ba and their oxides, J. Electron. Spectrosc. Relat. Phenom. 21 (1980) 265–273, https://doi.org/10.1016/0368-2048(80)85055-9.

[40] A. Cavallaro, G.E. Wilson, G. Kerherve, E. Cali, C.A.M. van den Bosch, P. Boldrin, D. Payne, S.J. Skinner, A. Aguadero, Analysis of H2O-induced surface degradation in SrCoO3-derivatives and its impact on redox kinetics, J. Mater. Chem. A 9 (2021) 24528–24538, https://doi.org/10.1039/d1ta04174f.

[41] T.J. Chuang, C.R. Brundle, D.W. Rice, Interpretation of the x-ray photoemission spectra of cobalt oxides and cobalt oxide surfaces, Surf. Sci. 59 (1976) 413–429, https://doi.org/10.1016/0039-6028(76)90026-1.

[42] M. Oku, K. Hirokawa, X-ray photoelectron spectroscopy of Co3O4, Fe3O4, Mn3O4, and related compounds, J. Electron. Spectrosc. Relat. Phenom. 8 (1976) 475–481, https://doi.org/10.1016/0368-2048(76)80034-5.

[43] K.P. Reddy, R. Jain, M.K. Ghosalya, C.S. Gopinath, Metallic cobalt to spinel Co3O4-electronic structure evolution by near-ambient pressure photoelectron spectroscopy, J. Phys. Chem. C 121 (2017) 21472–21481, https://doi.org/10.1021/acs.jpcc.7b06661.

[44] G.F. Liu, P.P. Ma, Y. Qiao, R.H. Xu, D.M. Huang, R.Y. Hu, L.Y. Liu, G.H. Jiang, M. Demir, Perovskite SrCo1-xTixO3-δ as anion-intercalated electrode materials for supercapacitors, J. Energy Storage 52 (2022) 104942, https://doi.org/10.1016/j.est.2022.104942.

[45] A.P. Dementjev, O.P. Ivanova, L.A. Vasilyev, A.V. Naumkin, D.M. Nemirovsky, D. Y. Shalaev, Altered layer as sensitive initial chemical state indicator, J. Vac. Sci. Technol. A Vacuum, Surfaces, Film. 12 (1994) 423–427, https://doi.org/10.1116/1.579258.

[46] H. Sun, B. Hu, D. Guan, Z. Hu, L. Fei, M. Li, V.K. Peterson, H.J. Lin, C. Te Chen, R. Ran, W. Zhou, Z. Shao, Bulk and surface properties regulation of Single/Double perovskites to realize enhanced oxygen evolution reactivity, ChemSusChem 13 (2020) 3045–3052, https://doi.org/10.1002/cssc.202000704.